View metadata, citation and similar papers at core.ac.uk

brought to you by CORE

東北大学機関リポジトリ TOUR Tohoku University Repository

Self-multilayered structures of SiN films prepared by plasma-enhanced reactive sputtering

著者	桑野　博喜
journal or publication title	Journal of applied physics
volume	76
number	12
page range	8097-8104
year	1994
URL	http://hdl.handle.net/10097/35251

doi: 10.1063/1.357858

Self-multilayered structures of SiN films prepared by plasma-enhanced reactive sputtering

Iwao Sugimoto, Satoko Nakano,[a] and Hiroki Kuwano
NTT Interdisciplinary Research Laboratories, Midoricho, Musashino-shi, Tokyo 180, Japan

(Received 2 May 1994; accepted for publication 29 August 1994)

Nanometer structures are fabricated with SiN films prepared by plasma-enhanced reactive sputtering using He and Ne Penning effects. These structures are characterized by microscopic and spectroscopic investigations. Films produced with He-N_2 and with Ne-N_2 gases consist of multilayered structures with columnar and equiaxed layers even though the sputtering conditions are kept constant. The equiaxed layers, which tend to be thin and stressed, are resistant to chemical etching using buffered hydrogen fluoride (BHF) because of the oxygen- and hydrogen-poor structures, whereas the columnar layers consisting of oxygen-rich components are thick and easily etched. The He-N_2 film with thickness more than 2 μm basically consists of a simple two-layered structure: a thick columnar layer beneath an equiaxed thin top layer. BHF etching forms closely packed bundles of SiN fibers with mean thickness of 10 nm. The Ne-N_2 film consists of a multilayered structure with many layers with thin equiaxed layers inserted between thick columnar layers. The multilayered structure is probably due to two different surface temperatures that were used for depositing alternate layers. The combination of these two complementary structures provides the useful characteristics of high chemical etching resistivity and low film stress. © *1994 American Institute of Physics.*

I. INTRODUCTION

In micromachining technology, the increasing usefulness of hard nitride films for constructing microscale structures and surface coatings, which are used as corrosion-, oxidation-, and wear-resistant films, brings with it the need for advanced characterization of film structure.[1–7] A variety of optical, electrical, and mechanical testing procedures has been used to provide information about the characteristics of these films. Microstructural characterization of chemical bonding and atomic states is principally achieved by spectroscopic investigation, and morphological insights are primarily obtained by the electron and scanning microscopies. Film morphology substantially reflects the bonding style of the film constituents. Combined understanding of both microscopic and macroscopic perspectives should be effective in obtaining a clear description of film characteristics.

During construction of film frameworks, the film constituents are likely to undergo physical, chemical, and thermal effects in the plasmas. In the case of reactive plasma techniques that have many interacting parameters, the origin in the film morphology is very complicated and cannot be simplified. According to the structure zone model (SZM) for sputtering deposition, the most important factors governing the film morphology are the mobility of the film precursor on the top surface and the flux of plasma particles impinging on the substrate.[8–12] In addition, chemical reactivity of the arriving particles on the top surface also plays a significant role in constructing the film structure in reactive plasma deposition techniques.

Silicon nitride (SiN) films have been widely investigated especially using chemical-vapor-deposition (CVD) methods; however, CVD methods have the intrinsic disadvantages of high processing temperature and inclusion of heteroatoms originated in the undecomposed chemical bonds in the raw molecules.[13–16] On the other hand, sputtering methods are likely to provide unstoichiometric films due to selective nitrogen elimination and low nitridation reactivity. Concerning to the residual film stress, CVD films tend to have tensile stress and the sputtered films tend to have compressive stress.

We have previously reported plasma excitation methods using He Penning effects to enhance the nitridation reactivity during magnetron sputtering.[17] This method can provide extremely low-stress films without post-treatment. The present study enlarges upon existing information regarding the nature of nanometer structures of the SiN films produced by plasma-enhanced sputtering using He and Ne gases. The multilayered structures can be obtained even though the sputtering conditions are kept constant. These prominent structures consist of columnar and equiaxed layers and play substantial roles in film characteristics.

II. EXPERIMENTATION

A. Film preparation

SiN films were prepared by using planar-diode-type rf (13.56 MHz) magnetron sputtering equipment with sputter-up configuration (Anelva, SPF-312H). The substrate, an undoped ⟨100⟩ silicon wafer, was held on the grounded electrode and kept at 50 °C. A 150 mm single-crystal silicon disk on the lower electrode was connected to the 13.56 MHz rf power supply. The power density was 2.83 W/cm^2 and the interelectrode distance was 50 mm. The background pressure before deposition was always 8×10^{-6} Pa by using the combination of a diffusion pump (600 ℓ/s) and a liquid-nitrogen trap, and the sputtering pressure was kept at 2 Pa. The gas

[a]NTT Advanced Technology Corporation, 3-9-11, Midoricho, Musashino-shi, Tokyo 180, Japan.

 0021-8979/94/76(12)/8097/8/$6.00 © 1994 American Institute of Physics

Downloaded 15 Oct 2008 to 130.34.135.158. Redistribution subject to AIP license or copyright; see http://jap.aip.org/jap/copyright.jsp

ratio between nitrogen and inert gases was determined by their flow rates controlled by mass flow controllers (Brooks 5877).

Sputtered SiN films prepared in excited plasma using He and Ne gases consist of highly saturated Si-N networks and have low internal film stress. Spectroscopic analysis has revealed that this plasma-excitation effect by He and Ne Penning effects is prominent when the plasma–working-gas mixture ratio of nitrogen and noble gases is above nine [$He(Ne)/N_2>9$].[18] In addition to the chemical bonds in Si-N networks, the plasma excitation should profoundly affect the microstructure of the resultant SiN films by improving their mechanical and chemical characteristics. Therefore, we focused on revealing the nanometer morphology corresponding to the chemical structure of the films produced in the $He(Ne)/N_2=9$.

Chemical etching is an effective post-treatment for obtaining the morphological features of hard nitride films. Chemical etching for the sputtered SiN films was performed using buffered hydrogen fluoride (BHF) solution ($HF:NH_4F=1:7$) at 20 °C. The chemical etching characteristics were estimated by measuring step heights between the Cr-masked (100 Å thick) and bare surfaces.

B. Characterization

Film morphology was observed by scanning electron microscopy (SEM, JEOL JSM-300) and transmission electron microscopy (TEM, Hitachi H-9000), which operated at 250 kV allowing a spatial resolution of about 0.2 nm. Specimens for TEM analysis were obtained by using the standard technique: attaching a dummy silicon wafer, cutting, polishing, dimpling, and ion etching. Both sides of the silicon wafer were ion etched using an Ar^+ beam with incident angle of about 15°.

Profiles of the film components were analyzed by secondary-ion-mass-spectroscopy (SIMS) using a magnetic sector-type mass spectrometer (Cameca IMF-4F). 14.5 keV Cs^+ ions were used for the probing beam and the ion current was 10 nA. The operating pressure during mass analysis was kept below 10^{-7} Pa. The focused ion beam was raster scanned over an area of 125×125 μm while secondary ions were collected from a circular area (60 μm in diameter) in the center of the raster-scanned region.

Using the cleaved samples, the cross-sectional distribution of the film constituents was determined by electron probe microanalysis (EPMA, JEOL JXA-8600). All of the samples were coated with carbon to prevent charging. The applied voltage to accelerate the probing electrons was 15 kV and the electron-beam current was 5×10^{-8} A. Elements with atomic numbers greater than carbon were detectable by using four x-ray analyzing crystals [LiF (lithium fluoride), PET (pentaerythriol), TAP (thallium acid phtharate), LDE (layered dispersion element)1]. The background pressure in the chamber was below 10^{-6} Torr and the signal sampling area was about 1 μm in diameter.

Chemical bonding and diffraction analysis were carried out by Fourier transform infrared (FTIR) spectroscopy. This analysis was performed using a JASCO FT/IR-5M with a microscope equipment (MICRO-10) that used a Cassegrain-type focusing system. The IR irradiation was restricted to 670×670 μm and the signal transmitted through samples was detected by a Hg-Cd-Te detector with a wave-number resolution of 4 cm^{-1}.

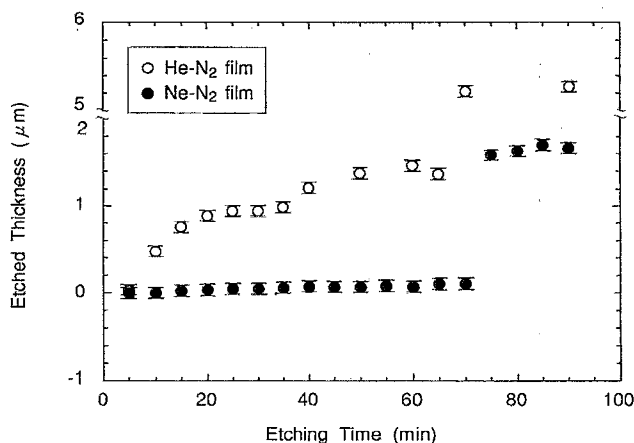

FIG. 1. BHF-etched film thickness varying etching time.

III. RESULTS AND DISCUSSION

The BHF-etched thickness of the SiN films varying etching time is shown in Fig. 1. The original film thickness for the $He-N_2$ film was 5.2 μm and for the $Ne-N_2$ film it was 7.2 μm. The $He-N_2$ film shows that its etching characteristics clearly depend on time. That is, the etched thickness increased rapidly after 5 min, which is presumably due to the removal of the top resistive surface. Then, two exponential curves were observed from 5 to 35 min and 35–65 min. This suggests that there are two stages, in which each of these curves becomes more resistive to etching as etching time increases. At the end of the second stage, the remaining film was estimated to be about three-fourths of the film before etching. After 70 min, the film was suddenly etched away. We conclude that the $He-N_2$ film is composed of two parts: a thin durable part near the top surface below 1.3 μm and a thick fragile part underneath the durable top layer. On the other hand, the $Ne-N_2$ film is only slightly etched up to 70 min and the etching rate was estimated at 17 Å/m irrespective of etching time. The resistive surface layer of the $Ne-N_2$ film seemed to be removed at 75 min and the fragile layer underneath was etched away; however, one-fourth of the $Ne-N_2$ film remained after 90 min etching. In general, the $He-N_2$ film seemed to be etched and the $Ne-N_2$ film to be highly resistant to BHF etching.

However, these measurements of the etched thickness merely reflect the etching resistance to the removal of film components in the direction of film thickness. Cross-sectional SEM analysis provides detailed information about the etching behavior including side etching at the cleaved film surface. This analysis is especially informative for films with multilayered structure. SEM photographs illustrating the etching characteristics and microstructure of the $He-N_2$ film for various etching times are shown in Fig. 2. The whole structure of the as-deposited film can be explained using the

Downloaded 15 Oct 2008 to 130.34.135.158. Redistribution subject to AIP license or copyright; see http://jap.aip.org/jap/copyright.jsp

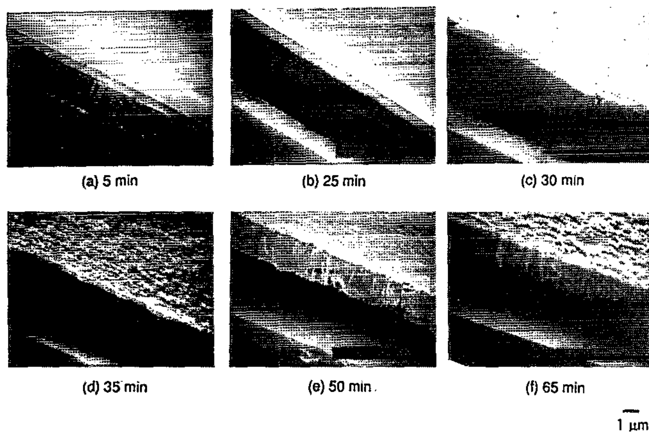

FIG. 2. BHF-etched He-N_2 film features for various etching times.

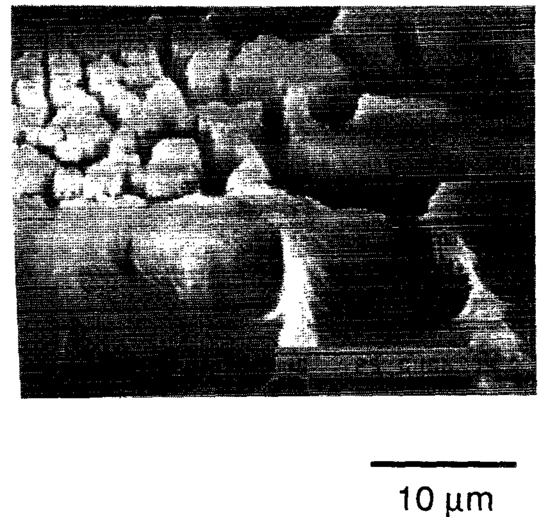

FIG. 3. Finely packed fibers produced by BHF etching of He/N_2=25 film.

slightly etched specimen [Fig. 2(a)]. In accordance with the results for the etched thickness (Fig. 1), the He-N_2 film generally consisted of two categories of film components: The equiaxed surface layer is about one-fourth of the total film thickness and the rest is a columnar layer. We observe that both of them are divided into several layers. From the 25 min etched specimen, we observe that the side etching of the columnar layers is greater than the surface etching of the equiaxed surface layer [Fig. 2(b)]. The surface equiaxed layer became thinner and rougher due to the residue of the equiaxed layer remaining even after the 30 min etching [Fig. 2(c)]. At 35 min, the equiaxed first surface layer almost disappeared and the second equiaxed layer began to be etched [Fig. 2(d)] at 35 minutes. After 50 min etching, the lower part of the columnar layer attached to the substrate was considerably side etched [Fig. 2(e)]. Even though it was highly resistive to etching, the equiaxed second layer almost completely vanished at 65 min [Fig. 2(f)]. The remaining columnar structures without protective equiaxed layers were suddenly etched away after 70 min etching. These results indicate that the equiaxed layers are strongly resistive to BHF etching and the columnar layers are fragile. Using a He-N_2 film produced in the He/N_2=25 plasma, we obtained closely packed fibrous nanometer structures (Fig. 3) with mean thickness of 10 nm.

The Ne-N_2 film also consisted of two kinds of film components: equiaxed and columnar layers (Fig. 4); but, in this case, the equiaxed layers were thinner and separately inserted into the columnar layers that contained several nodules. This is clearly identified after 15 min etching [Fig. 4(a)]. As in the He-N_2 film, the columnar layers are preferentially etched; however, the etching durability seems to be increased, compared with the He-N_2 film. In particular, the short densely packed columns attached to the substrate are nearly intact when the upper columnar layers are thinned out after 25 min etching [Fig. 4(b)]. We observed holes surrounded by corrugated strips spreading radially (Fig. 5). This pattern is probably due to the internal film stress, and the formation of these holes is probably initiated by the removal of the nodular structures.[19,20] The equiaxed top layer becomes thinner and rougher after the 65 min etching [Fig. 4(c)]. The upper layer then partially sinks resulting in a large number of holes after 75 min etching [Fig. 4(d)]. Finally, the upper columnar layers containing a thin equiaxed layer disappear after 85 min etching [Fig. 4(f)]. The large difference in etching rate between the He-N_2 and Ne-N_2 films (Fig. 1) is mainly due to the etching durability of the columnar layers directly attached to the substrate. Conventional sputtered SiN films produced in pure N_2 and Ar-N_2 plasmas consist only of an equiaxed layer with high internal film stress. On the other hand, we found that plasma-enhanced sputtering using He and Ne Penning effects produces multilayered structures with a combination of columnar and equiaxed layers. This multicomponent structure should play an important role in reducing the internal film stress[21] and in maintaining high resistivity to etching. Using the 4-μm-thick films, we fabricated 20-μm-wide microcross beams. The beam formed from pure N_2 cracked and broke due to high internal film stress, but the beams formed from He-N_2 and Ne-N_2 maintained their cross-beam structures even though they were slightly deformed downward (Fig. 6).

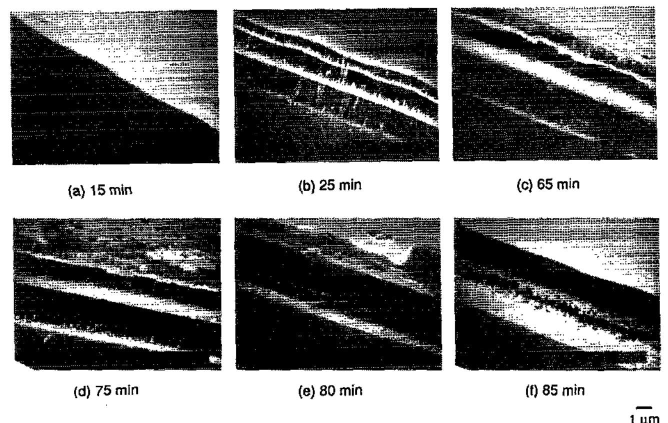

FIG. 4. BHF-etched Ne-N_2 film features for various etching times.

Downloaded 15 Oct 2008 to 130.34.135.158. Redistribution subject to AIP license or copyright; see http://jap.aip.org/jap/copyright.jsp

FIG. 5. BHF-etched hole produced on the Ne-N_2 film surface.

X-ray-diffraction analysis suggests amorphous structures for both films without any periodical structure.[17] Electron-diffraction analysis shows hollow patterns, also indicating that these films have amorphous structure. High-resolution cross-sectional TEM images for the He-N_2 and Ne-N_2 films are shown in Fig. 7. They show that both films contain a large number of bright stripes, whose sizes are larger for the Ne-N_2 film than for the He-N_2 film. We think that the bright stripes represent the lines of voids and intercolumnar boundaries because their direction of propagation is the same as for the columnar structure. The formation of these bright stripes may be due to shadowing effects[22–26] or trapping of the unreacted plasma species, such as He or Ne gas. High-resolution images show that the bright stripes are made up from aligned bubblelike components, whose diameter is less than 10 nm (Fig. 8) even for the Ne-N_2 film. We think that the columnar structures showed poor resistivity to BHF etching because the intercolumnar boundaries are eroded by exposure to etchants; however, the columnar structures probably play crucial roles in reducing the internal film stress.

The depth profiles of film constituents were analyzed by SIMS (Fig. 9). We prepared other specimens for BHF-etching analysis. By comparing the slightly BHF-etched specimens, we found that the equiaxed surface layer was

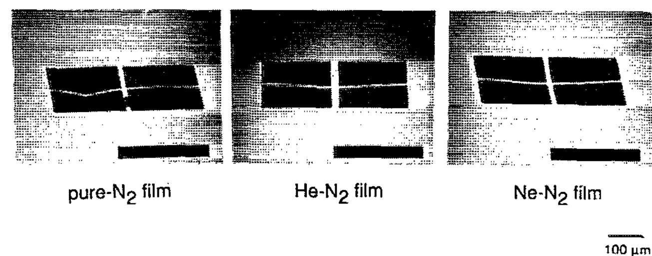

FIG. 6. Free-standing microcross beams using SiN films prepared in the pure N_2, He-N_2, and Ne-N_2 plasmas.

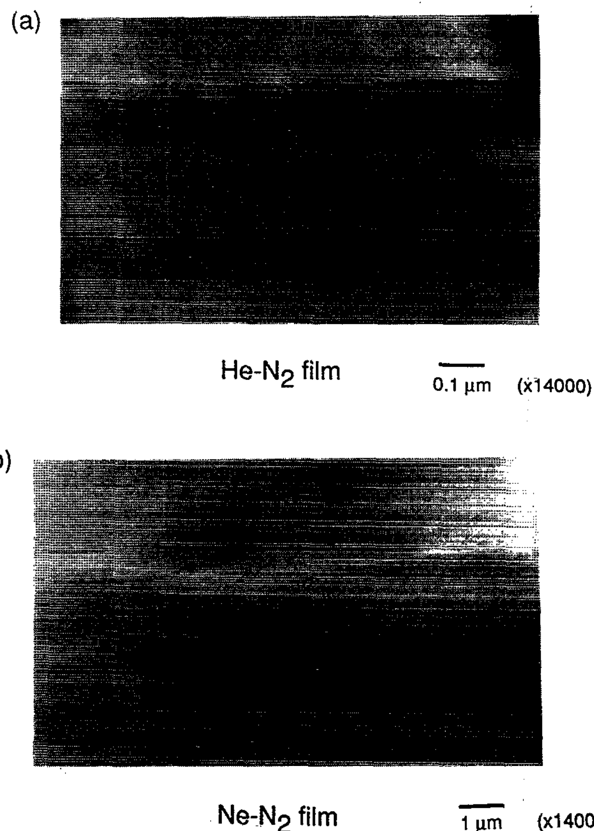

FIG. 7. Cross-sectional TEM images: (a) He-N_2 film; (b) Ne-N_2 film.

thinner for this He-N_2 film [Fig. 10(a)]; however, the basic structure was identical for both He-N_2 films which consisted of columnar structures. The Ne-N_2 films had the same structure with a complicated combination of equiaxed and columnar layers, even though the location, thickness, and number of equiaxed layers were slightly changed [Fig. 10(b)]. All of the species were detected as negative ions to reduce background interference. The silicon and oxygen profiles are clearly observable in Fig. 9 as the profiles of the rare isotopes (^{30}Si and ^{18}O). The nitrogen profile can be expressed in terms of the NSi_2^- molecular ion profile because the silicon distribution is almost uniform.

Both films show a slight decrease in silicon and nitrogen atom intensity with increase in etching depth. Besides the film constituents (Si and N atoms), oxygen and hydrogen atoms were detected. They must have been incorporated through plasma reactions with residual contamination gases, such as water and oxygen molecules.[27] For the He-N_2 film, the atomic density of nitrogen and oxygen increased at the film-substrate interface. The oxygen enrichment near the film-substrate interface may be caused by the surface oxide layer of the silicon substrate. Moreover, the concentration of hydrogen and oxygen atoms is reduced at depths below 0.4 μm from the film surface. Comparing the film morphology [Fig. 10(a)], this hydrogen- and oxygen-deficient area corresponds to the equiaxed layer located at the film surface.

Comparing secondary ion counts of both film constituents, the nitrogen background level of the Ne-N_2 film is

Downloaded 15 Oct 2008 to 130.34.135.158. Redistribution subject to AIP license or copyright; see http://jap.aip.org/jap/copyright.jsp

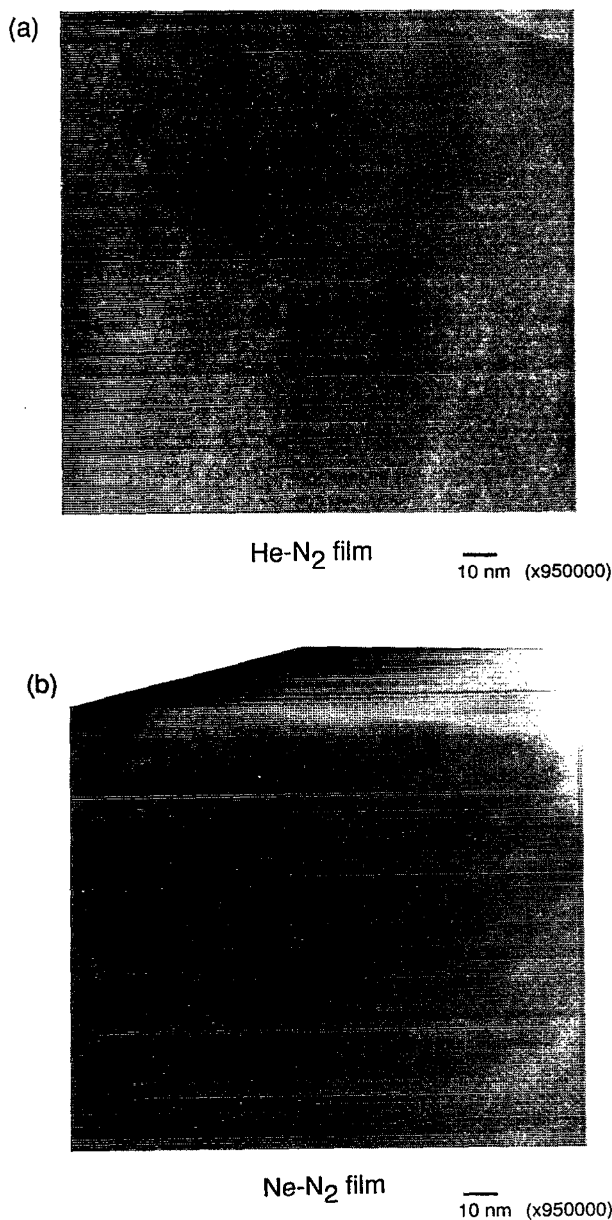

FIG. 8. High-resolution cross-sectional TEM images: (a) He-N_2 film; (b) Ne-N_2 film.

larger than that of the He-N_2 film; however, the Ne-N_2 film does not show a nitrogen-rich profile at the film-substrate interface. Oxygen enrichment at the film-substrate interface is likely as with the He-N_2 film. This Ne-N_2 film has the characteristic profiles of hydrogen and oxygen atoms. Their signal intensities change synchronously suggesting that there are several oxygen- and hydrogen-deficient layers. Comparing the SIMS profile [Fig. 9(b)] with the SEM photograph [Fig. 10(b)], these less-contaminated layers correspond to the equiaxed layers as described for the He-N_2 film. Taking into account the high resistivity to BHF etching, these equiaxed layers are composed of oxygen- and hydrogen-deficient components. These results suggest that columnar layers contain inevitable contaminant oxygen and hydrogen atoms and the equiaxed layers are less contaminated.

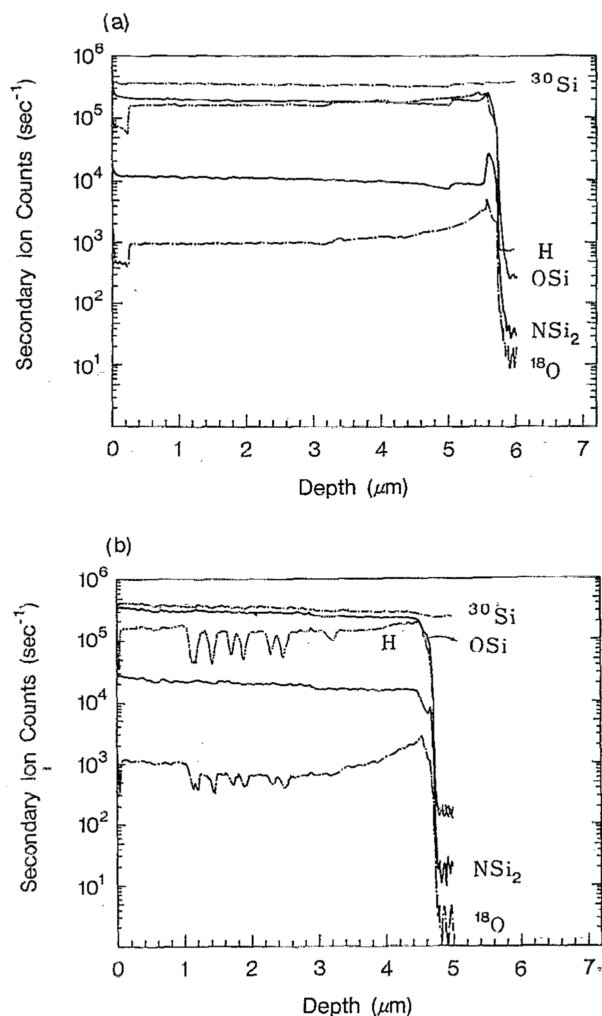

FIG. 9. Depth profiles of film constituents analyzed by SIMS: (a) He-N_2; (b) Ne-N_2 film.

We also determined elemental depth profiles by cross-sectional EPMA for both samples used in the SIMS analysis (Fig. 10). Besides silicon and nitrogen atoms, EPMA also revealed that oxygen atoms take part in forming both the He-N_2 and Ne-N_2 film frameworks, even though the He-N_2 film was BHF etched for 13 min and the Ne-N_2 film was BHF-etched for 13 min. Atomic ratios for the He-N_2 and

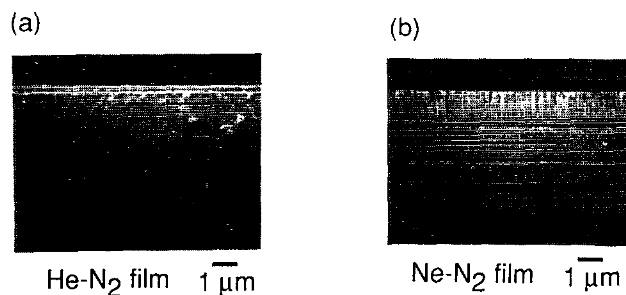

FIG. 10. Cross-sectional view of SiN films used for SIMS analysis; (a) He-N_2 film; (b) Ne-N_2 film.

Downloaded 15 Oct 2008 to 130.34.135.158. Redistribution subject to AIP license or copyright; see http://jap.aip.org/jap/copyright.jsp

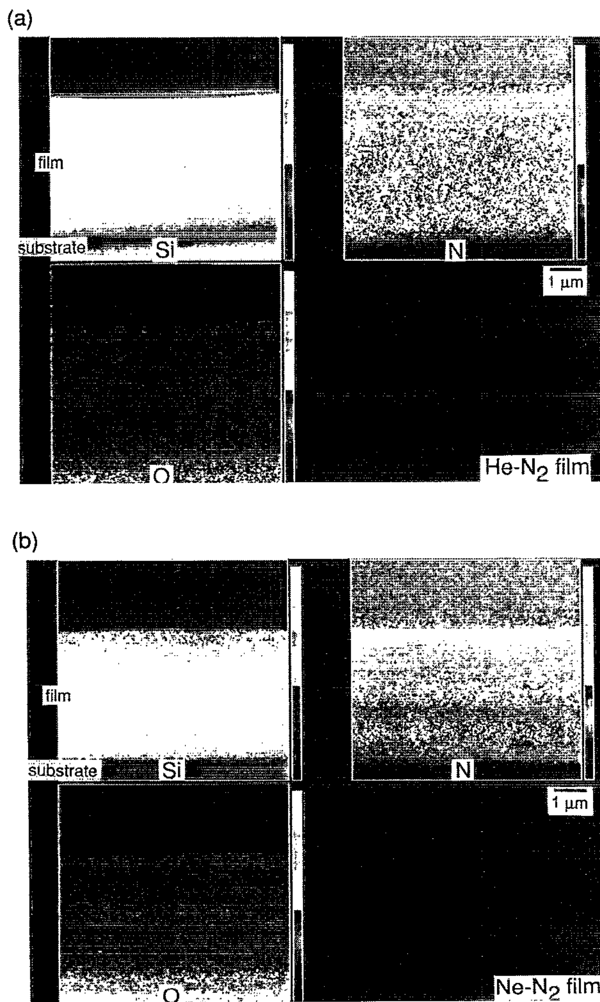

FIG. 11. Cross-sectional elemental mapping obtained by EPMA: (a) He-N_2 film (BHF etched for 13 min); (b) Ne-N_2 film (BHF etched for 30 min).

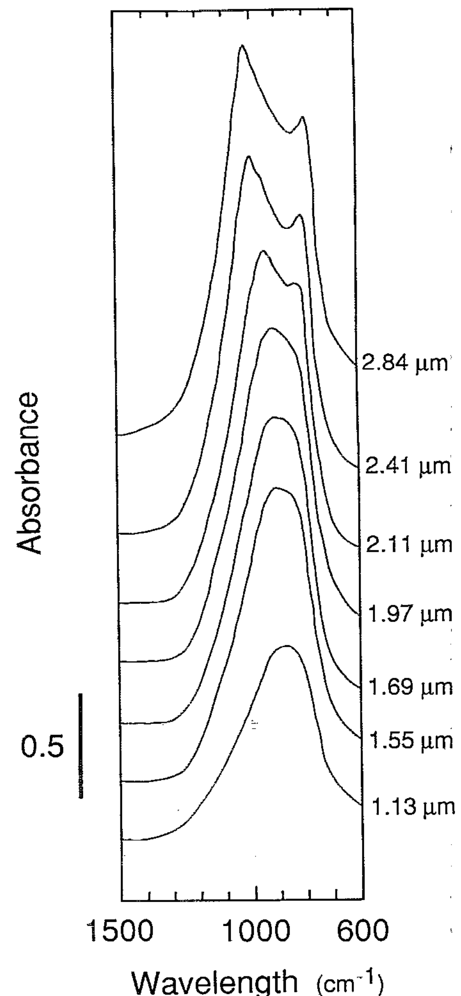

FIG. 12. Si-N stretching band changes for various He-N_2 film thicknesses.

Ne-N_2 films were evaluated at Si:N:O=43.53:4 and Si:N:O =44:55:1. Cross-sectional views of the elemental mapping are shown in Fig. 11 in order to compare the morphology and elemental distributions revealed by SEM and SIMS analyses. Taking into account the spatial signal resolution, no elemental distribution structures are detectable for the He-N_2 film. On the other hand, the Ne-N_2 film has a nitrogen-rich structure near the Ne-N_2 film surface. As with the SIMS analysis for the Ne-N_2 film, we observe synchronous changes between nitrogen-poor and oxygen-rich layers distributed near the film substrate. Based on the 1 μm spatial resolution, the nitrogen enrichment without fine structure near the Ne-N_2 film surface is probably caused by the overlapping of the stronger nitrogen signals from the equiaxed layers whose interlayer distance is less than 1 μm. Compared with the morphological SEM analysis, these SIMS and EPMA investigations show that the thin equiaxed layers consist of oxygen-poor and nitrogen-rich components, which are chemically inert and mechanically strong.

In general, the He-N_2 film has a simple bilayer structure, that is, the thick columnar layer is covered with a thin equiaxed layer. From SEM analysis we found that the development of the surface equiaxed layer is greatly affected by total film thickness. The He films with thickness less than about 2 μm consisted of only a columnar layer without the surface equiaxed layer. We therefore investigated the growth of the equiaxed layer by FTIR spectroscopy. Besides providing atomic bonding information, FTIR spectroscopy gives information about multilayered structures which produce interference signals. Figure 12 shows the Si-N stretching bands for various thicknesses of He-N_2 film. The absorbance increases with increasing film thickness. Over 2 μm thick, we observe the inversion of the upper part of the band at a center of 895 cm^{-1}. This inversion of the Si-N band is induced by interference between the refracted signals through the multilayered structure.[28,29] Therefore, we estimate that the development of the surface equiaxed layer becomes noticeable for films with total film thickness over 2 μm. This structural information is also important for practical applications.

Based on the SZM which explains the sputtered film microstructures, we deduce the mechanism for constructing the alternate structures of the equiaxed and the columnar layers for the He-N_2 and Ne-N_2 films (Fig. 13). The maximum process temperature was measured with a thermal in-

Downloaded 15 Oct 2008 to 130.34.135.158. Redistribution subject to AIP license or copyright; see http://jap.aip.org/jap/copyright.jsp

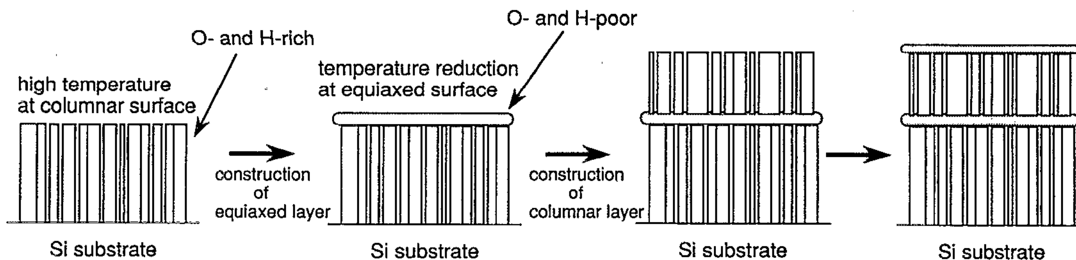

FIG. 13. Schematic mechanism for constructing the alternate structures between the columnar and equiaxed layers for $He-N_2$ and $Ne-N_2$ films.

dicator label directly attached to the substrate. When the film thickness was about 1 μm, the maximum substrate temperature was about 160 °C irrespective to the plasma–working-gas composition. This maximum substrate temperature increases to over 300 °C when the film thickness is increased to 2 μm. According to the SZM, the former temperature is less than the critical value T_c for oxides or nitrides, i.e., $0.2<T_s/T_m<0.3$ at 2 Pa (T_s: substrate temperature; T_m: melting point of SiN, assumed to be 1500 °C) which is the criterion for deciding between the equiaxed and columnar structures.[8–12] For film thickness below 2 μm, the surface migration of the film components was sufficiently reduced to allow the columnar structure to be formed (zone 1 or T) under conditions of low temperature ($T_s/T_m<T_c$) and low gas pressure (2 Pa in this study). As the film thickness increased, the temperature of the top surface of the deposited film increased due to the insulating effect of the SiN film. Therefore, the surface temperature exceeded T_c and the mobility of the film components increased, thus changing the columnar structure of the equiaxed structure. This increase in surface temperature should change the morphology to an equiaxed layer growing on a columnar layer. The increase in saturation of Si-N networks caused by He and Ne Penning effects[17] may inherently contribute to the construction of the columnar structures which is unique for $He-N_2$ and $Ne-N_2$ plasma products.

The morphological difference between the $He-N_2$ and $Ne-N_2$ films may be due to the difference in thermal conductivity of the plasmas which produce these films. This inference is based on the fact that films prepared in pure N_2 and $Ar-N_2$ mixture gases consist only of equiaxed structures. He and Ne gases can reduce the temperature of the N_2 plasma by mixing with them because their atomic weights are lower than the molecular weight of N_2, so they increase the thermal conductivity of the gas mixture plasmas.[30] Ar gas, however, does not have this N_2 plasma gas cooling effect. He is more effective than Ne in reducing the temperature of N_2 gas plasma. Therefore, the rate of increase of plasma temperature is higher for $Ne-N_2$ plasma and the equiaxed layer appears faster than with $He-N_2$ plasma. In the course of developing the equiaxed layer, the temperature of the top surface should be reduced again to the temperature needed to form the columnar structure ($T_s/T_m<T_c$) by effective thermal radiation of the densified equiaxed structures. The $Ne-N_2$ films had several thin layers forming multilayered structures, because the temperature of the growing top surface was changed alternately at short intervals between the equiaxed and columnar temperatures. Moreover, the period of this change decreased with increase in film thickness due to the reduction in the cooling ability of the thicker insulating SiN film. Therefore, the interlayer distance between the equiaxed layers tends to become smaller as they approach the resulting film surface. These results show that the equiaxed layers have oxygen- and hydrogen-deficient structures because these contamination species have shorter residence time at higher surface temperatures.

IV. CONCLUSIONS

We discussed the nanometer structures of SiN films produced by highly reactive magnetron sputtering using He and Ne gases which enhance the nitridation reactivity through Penning effects. SEM and TEM analyses in combination with elemental depth profiling using SIMS and EPMA revealed microstructural features of the resulting films that correlated with the elemental distribution. BHF-etching characterization showed that these $He-N_2$ and $Ne-N_2$ plasmas preferentially form columnar layers which do not occur when using conventional pure N_2 and $Ar-N_2$ plasmas because of the high thermal conductivity of the $He-N_2$ and $Ne-N_2$ plasmas. The columnar layers are easily etched due to the hydrogen- and oxygen-rich and voidous structures. Using a $He-N_2$ film that was mainly composed of the fine columnar structure, we prepared closely packed bundles of SiN fibers by BHF etching. The other products of the $He-N_2$ and $Ne-N_2$ plasmas were thin equiaxed layers which were stressed and resistant to BHF etching due to the hydrogen- and oxygen-poor structures. The $He-N_2$ films are likely to have a simple bilayer structure; a thin equiaxed layer develops at the film surface encapsulating the thick columnar layer underneath. By analyzing interference signals from $He-N_2$ films by FTIR spectroscopy, we identified the formation of this equiaxed layer in $He-N_2$ films with thickness over 2 μm. On the other hand, the $Ne-N_2$ film consisted of multilayered structures in combination with equiaxed and columnar layers. SZM showed that this self-multilayered structure is caused by the alternating changes in surface temperature during development of the $Ne-N_2$ film. These $He-N_2$ and $Ne-N_2$ films should be useful for microstructural films with low internal film stress and high durability against chemical etching.

Downloaded 15 Oct 2008 to 130.34.135.158. Redistribution subject to AIP license or copyright; see http://jap.aip.org/jap/copyright.jsp

ACKNOWLEDGMENTS

The authors would likely to thank Keiichi Yanagisawa for his technical support in fabricating the microcross beams and for useful discussions.

[1] S. J. Bull, Vacuum **43**, 387 (1992).
[2] R. Luthier and F. Levy, J. Vac. Sci. Technol. A **9**, 102 (1991).
[3] H. Windischmann, J. Vac. Sci. Technol. A **9**, 2431 (1991).
[4] P. A. Beck, S. M. Taylor, J. P. Mcvittie, and S. T. Ahn, Mater. Res. Soc. Symp. Proc. **182**, 207 (1990).
[5] F. M. D'Heurle and J. M. E. Harper, Thin Solid Films **171**, 81 (1989).
[6] D. S. Rickerby and P. I. Burnett, Thin Solid Films **157**, 195 (1988).
[7] R. F. Bunshah and C. V. Deshpandev, Vacuum **39**, 955 (1989).
[8] J. A. Thornton, Ann. Rev. Mater. Sci. **7**, 239 (1977).
[9] J. A. Thornton, J. Vac. Sci. Technol. A **4**, 3059 (1986).
[10] J. A. Thornton and D. W. Hoffman, Thin Solid Films **171**, 5 (1989).
[11] B. A. Movchan and A. V. Demchishin, Phys. Met. Metallogr. **28**, 83 (1969).
[12] R. Messier, A. P. Giri, and R. A. Roy, J. Vac. Sci. Technol. A **2**, 500 (1984).
[13] L. F. Cordes, Appl. Phys. Lett. **11**, 383 (1967).
[14] C. J. Mogab and E. Luguijo, J. Appl. Phys. **47**, 1302 (1976).
[15] X. Qui and E. Gyarmati, Thin Solid Films **151**, 223 (1987).
[16] T. Carrier, I. Vickridge, B. Agius, P. Alout, J. Siejka, and R. Joubard, Plasma Processing **PV88-22**, 370 (1987).
[17] I. Sugimoto and S. Nakano, Appl. Phys. Lett. **62**, 2116 (1993).
[18] I. Sugimoto, S. Nakano, and H. Kuwano, J. Appl. Phys. **75**, 7710 (1994).
[19] T. Spalvins and W. A. Brainard, J. Vac. Sci. Technol. **11**, 1186 (1974).
[20] K. H. Guenther, Appl. Opt. **20**, 1034 (1981).
[21] P. Chaudhari, J. Vac. Sci. Technol. **9**, 520 (1971).
[22] D. Henderson, M. H. Brodsky, and P. Chaudhari, Appl. Phys. Lett. **25**, 641 (1974).
[23] A. G. Dirks and H. J. Leamy, Thin Solid Films **47**, 219 (1977).
[24] K.-H. Muller, J. Appl. Phys. **62**, 1796 (1987).
[25] P. J. Martin, Vacuum **36**, 585 (1986).
[26] G. S. Bales and A. Zangwill, J. Vac. Sci. Technol. A **9**, 145 (1991).
[27] A. Markwitz, H. Baumann, E. F. Krimmel, M. Rose, K. Bethge, P. Misaelides, and S. Logothetidis, Vacuum **44**, 367 (1993).
[28] W. N. Hansen, J. Opt. Soc. Am. **58**, 380 (1968).
[29] R. A. Dluhy, M. L. Mitchell, T. Pettensky, and J. Beers, Appl. Spectrosc. **42**, 1289 (1988).
[30] H. M. Jenning, B. J. Dalgleish, and P. L. Pratt, J. Mater. Sci. **23**, 2573 (1988).

Downloaded 15 Oct 2008 to 130.34.135.158. Redistribution subject to AIP license or copyright; see http://jap.aip.org/jap/copyright.jsp